High-resolution 3D Inspection of Bonding Defects in HBM using Optically-coupled X-ray Computed Laminography

Jaeyoung Im, Minjun Kim, and Sung Oh Cho*
Korea Advanced Institute of Science & Technology (KAIST)
Department of Nuclear and Quantum Engineering, Korea Advanced Institute of Science and Technology (KAIST), 291 Daehak-ro, Yuseong-gu
Daejeon 34141, Republic of Korea
Ph: 042-350-3863; Fax:-
Email: socho@kaist.ac.kr

Abstract

The rapid growth of artificial intelligence and high-performance computing has accelerated demand for high-bandwidth memory (HBM), in which dozens of DRAM dies are vertically stacked and interconnected through through-silicon vias (TSVs) and micro-bumps. Bonding defects such as bump voids, non-wets, and misalignment in these interconnects critically affect device yield and reliability, making nondestructive three-dimensional (3D) inspection essential. Conventional X-ray imaging systems rely on geometric magnification, which forces the use of low-power nano- or micro-focus sources and results in scan times exceeding 30 minutes per HBM module. In this work, we present an optically-coupled X-ray computed laminography (CL) system that decouples spatial resolution from the X-ray focal spot size by placing a scintillator in direct contact with the object and acquiring images through an optical magnification stage. This configuration allows the use of a high-power X-ray tube with a large focal spot without sacrificing resolution. A sub-micrometer spatial resolution was achieved using a 11-μm-thick CsI:Tl scintillator and a 10× optical lens, and 3D reconstruction of an HBM module from 1600 projections clearly resolved DRAM-to-DRAM and DRAM-to-logic micro-bumps along with bump voids. The proposed system establishes a practical route toward high-throughput, high-resolution in-line inspection of advanced 2.5D/3D semiconductor packages.

Key words

X-ray computed laminography, high-bandwidth memory, optical magnification, nondestructive inspection, semiconductor packaging

I. Introduction

The proliferation of artificial intelligence (AI), high-performance computing (HPC), and large-scale data-center applications has driven an unprecedented demand for memory bandwidth. High-bandwidth memory (HBM), in which multiple DRAM dies are vertically stacked on a logic die and interconnected by through-silicon vias (TSVs) and micro-bumps, has emerged as the dominant solution to satisfy this demand [1]. As the number of stacked DRAM layers continues to increase from HBM3 to HBM4 and beyond, the structural complexity and the number of interconnects per module rise rapidly, and the corresponding bonding processes become increasingly susceptible to defects.

Bonding defects such as micro-bump voids, non-wets, misalignment between dies, tilted or cracked TSVs, and warpage-induced interfacial gaps can severely degrade electrical performance, accelerate thermal-mechanical failure, and ultimately reduce module yield [2,3]. Because these defects are buried inside a sealed multi-die stack, they cannot be identified by external optical inspection or by electrical testing alone, which can only detect connectivity failures without localizing them. Nondestructive three-dimensional (3D) imaging of fully assembled HBM modules is therefore essential to ensure reliability and to provide actionable feedback to upstream bonding processes.

Among nondestructive techniques, X-ray computed tomography (CT) has been widely adopted for internal inspection of advanced packages because it can resolve micrometer-scale features without disassembly [4]. Conventional X-ray CT systems use geometric magnification, in which the magnification factor is determined by the ratio of the source-to-object distance (SOD, R_1) and the object-to-detector distance (ODD, R_2). To resolve micro-bumps and TSVs whose critical dimensions are on the order of tens of micrometers, a spatial resolution

of a few micrometers or better is required, which in turn demands a small X-ray focal spot to suppress geometric blurring.

Reducing the X-ray focal spot size, however, fundamentally limits the achievable tube power, because the electron-beam power that can be dissipated on the target anode scales with the focal spot area [5,6]. As a result, nano-focus and micro-focus X-ray tubes used for high-resolution package inspection typically operate at only a few watts, producing a very low X-ray flux. Acquiring hundreds of projection images at sufficient signal-to-noise ratio (SNR) then requires long exposure times, and a single HBM scan can take more than 30 minutes. Such throughput is incompatible with in-line inspection during high-volume manufacturing, where every module must be inspected within seconds to a few minutes.

To break this long-standing trade-off between spatial resolution and scan time, we have developed an optically-coupled X-ray computed laminography (CL) system. Computed laminography is a 3D imaging modality in which the rotation axis is inclined with respect to the X-ray beam, and it is particularly well suited for planar, plate-like samples such as HBM modules, printed circuit boards, and pouch-type batteries [7,8]. In the proposed system, a thin, high-resolution scintillator is placed in direct contact with the object so that the geometric magnification factor approaches unity, and image magnification is achieved purely by an optical lens. This configuration decouples spatial resolution from the X-ray focal spot size, enabling the use of a high-power X-ray tube with a large focal spot without compromising resolution. As a result, the per-projection exposure time and the total scan time can be reduced by more than an order of magnitude compared to conventional micro-focus CT.

II. Design of the Optically-Coupled X-Ray CL System

This section first describes how the optical-coupling configuration decouples spatial resolution from the X-ray focal spot size. It then analyzes the dominant factors that govern the achievable spatial resolution of the system, and finally summarizes the design choices made to optimize the system for HBM inspection.

A. Decoupling of X-Ray Focal Spot Size and Spatial Resolution

In a conventional X-ray imaging system that relies on geometric magnification (Fig. 1a), the magnification factor M is given by

$$M = (R_1 + R_2) / R_1, \qquad (1)$$

where R_1 is the SOD and R_2 is the ODD. The geometric blur B introduced by the finite X-ray focal spot size S scales as

$$B = S \cdot (R_2 / R_1) = S \cdot (M - 1). \qquad (2)$$

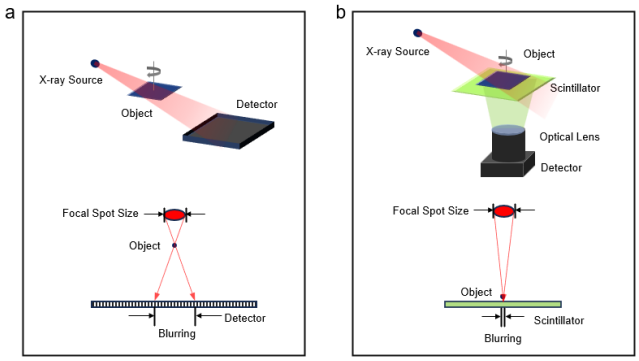


Figure 1. Comparison of X-ray imaging geometries and focal-spot-induced blurring. a) Conventional geometric magnification layout and blurring caused by the finite focal spot size of the X-ray source. b) Proposed optical magnification layout with blurring suppressed by direct contact with the scintillator.

To achieve high magnification, R_2 must be much larger than R_1, which inevitably amplifies the geometric blur from the focal spot. Suppressing this blur requires a small focal spot S, but the maximum X-ray power scales with the focal-spot area, since most of the electron-beam energy is dissipated as heat on the target anode. As S shrinks to a few micrometers, the deliverable power drops to the watt scale, the X-ray flux becomes very low, and the acquisition time per projection grows accordingly. In addition, very small focal spots are susceptible to focal-spot drift caused by localized thermal stress on the target, which introduces geometric errors during reconstruction and requires a stabilization interval before each scan [9].

In the proposed optically-coupled X-ray CL configuration (Fig. 1b), the X-ray detector is replaced by a thin scintillator placed in direct contact with the object, followed by an optical lens and an optical detector. Because the scintillator–object gap can be made on the order of a few hundred micrometers to a few millimeters, R_2 is much smaller than R_1 and the geometric magnification approaches unity:

$$M = 1 + R_2 / R_1 \approx 1 \quad (\text{when } R_2 \ll R_1). \qquad (3)$$

Substituting (3) into (2) shows that the geometric blur B approaches zero independently of S. Image magnification is then provided by the optical lens between the scintillator and the optical detector. This arrangement decouples the X-ray focal spot size from the spatial resolution, so that a high-power X-ray tube with a focal spot of several hundred micrometers can be used without degrading the achievable resolution, dramatically reducing the per-projection exposure time required for HBM inspection.

B. Spatial Resolution of the Optically-Coupled X-Ray Imaging System

Beyond suppressing source-induced geometric blur, the spatial resolution of the optically-coupled system is

governed by Fresnel diffraction during X-ray propagation, the residual source point spread function, the diffraction limit of the optical lens, the mismatch between the scintillator thickness and the depth of focus (DoF) of the optical system, and the effective pixel size of the camera [10–12]. The relevant terms are summarized below, with notation S, λ, λ', R_1, R_2, NA, M', e and n_scint denoting the X-ray focal spot size, the X-ray wavelength, the scintillator emission wavelength, SOD, ODD, the numerical aperture of the lens, the optical magnification, the camera pixel size, and the refractive index of the scintillator, respectively.

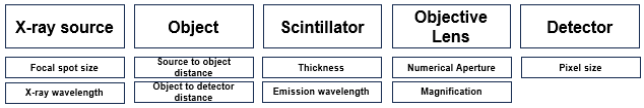


Figure 2. Major parameters influencing spatial resolution in the optically-coupled X-ray imaging system

$$R_{Fre} = (R'\lambda)^{1/2}, \quad R' = R_2 / M, \qquad (4)$$

$$R_{source} = \frac{S \cdot R_2}{2.4\, R_1}, \qquad (5)$$

$$R_{obj} = \frac{0.61\, \lambda'}{NA}, \qquad (6)$$

$$R_{scint} = \frac{(\Delta Z - DoF) \cdot NA}{2.4\, n_{scint}}), \qquad (7)$$

$$DoF = n\, \lambda' / NA + n\, e / (M'\, NA), \qquad (8)$$

$$R_{cam} = e / M'. \qquad (9)$$

R_{Fre} captures the Fresnel diffraction blur during free-space propagation from the object to the scintillator; it is intrinsically small in the proposed geometry because R_2 is short. R_{source} is the residual source PSF, whose Gaussian standard deviation is one-2.355th of the geometric blur in (2) [13]. R_{obj} is the Abbe diffraction limit of the optical lens and is set by NA at the scintillator emission wavelength λ'. R_{scint} accounts for out-of-focus blur when the scintillator thickness ΔZ exceeds the DoF of the optical system; choosing ΔZ ≤ DoF effectively eliminates this term for single-crystal or structured scintillators [14]. R_{cam} reflects the Nyquist limit imposed by the camera, where the effective pixel size at the object plane is e / M'.

For HBM inspection, micro-bumps and bump-void features of interest are typically on the order of tens of micrometers, while individual TSV diameters can be 5–10 µm. A spatial resolution near 1 µm is therefore desirable. Inspection of (4)–(9) shows that, once geometric blur has been suppressed by the optical-coupling configuration, the achievable resolution is dominated by the optical diffraction limit R_{obj} and the effective pixel size R_{cam}. These two terms are addressed by selecting a high-NA optical lens together with a high-magnification, low-pixel-pitch optical detector.

C. Development of the Optically-Coupled X-Ray CL System

In a conventional CT geometry, the rotation axis of the sample is parallel to the detector plane, which forces R_2 to be at least as large as the rotation radius of the object. For a planar object such as an HBM module, the long lateral dimensions of the package then make it difficult to bring the scintillator close to the region of interest. By adopting a laminography geometry, in which the rotation axis is inclined with respect to the detector, the scintillator can be placed very close to the planar object while still acquiring a full angular set of projections. In this configuration, the scintillator behaves as a virtual detector positioned at very small R_2.

Based on the spatial-resolution budget summarized above, the optically-coupled X-ray CL system was implemented as follows. A microfocus X-ray tube was operated at 100 kVp and 0.5 mA, and a 11-µm-thick CsI:Tl scintillator was placed in direct contact with the HBM module. CsI:Tl was chosen because its high effective atomic number and high density provide efficient absorption of the hard X-ray spectrum used for silicon-based packages, while its short decay time supports short per-projection exposures. The visible-light image emitted by the scintillator was relayed onto an sCMOS optical detector through a 10× microscope objective, yielding an effective pixel size of 0.64 µm at the object plane. With the sCMOS sensor and 10× objective, the corresponding field of view at the object plane was approximately 1.66 × 1.66 mm². Covering the full lateral extent of the HBM module (approximately 11 × 10 mm²) therefore requires a 7 × 6 array of tiled scans (42 scans in total), acquired by stepping the X–Y translation stage between adjacent fields. The sample stage was mounted on a precision rotary stage whose rotation axis was inclined with respect to the X-ray beam to satisfy the CL geometry.

The acquisition parameters used in this work are summarized in Table I. 1600 2D projection images were acquired over a rotation range of 368° with an exposure time of 0.5 s per projection. The 368° scan range extends beyond a full revolution to enable consistency checks and to mitigate truncation effects in the back-projection step. For the parameter set in Table I, the net exposure time was 800 s (1600 projections × 0.5 s), and the total acquisition time, including rotation and settling of the rotary stage between projections, was approximately 26 minutes.

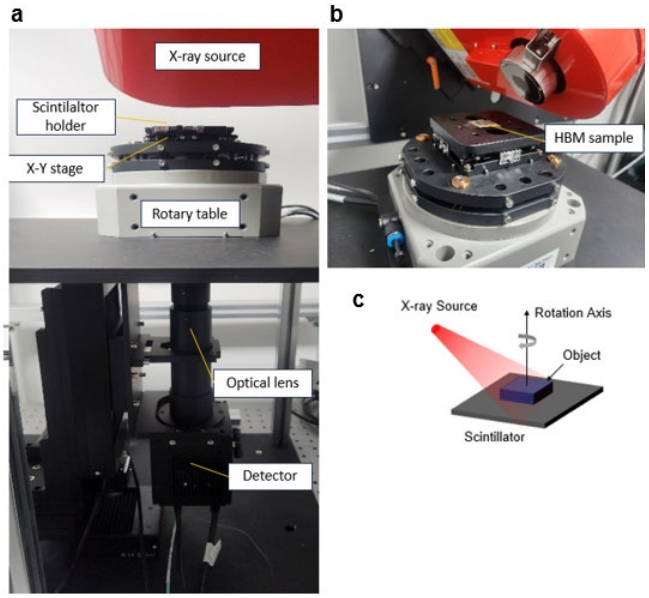


Figure 3. Developed optically-coupled X-ray CL system. (a) Photograph of the system showing the X–Y translation stage, rotary table, and scintillator holder. (b) Close-up of the HBM sample mounted on the rotary table. (c) Schematic of the imaging geometry.

Table I. Acquisition parameters used for HBM 3D imaging with the optically-coupled X-ray CL system.

Parameter	**Value**
Scintillator	CsI:Tl, 11 µm
Optical magnification	10×
Effective pixel size	0.64 µm
X-ray tube voltage / current (Power)	100 kVp / 0.5 mA (50 W)
X-ray focal spot size	50 µm
Scan angle	368°
Number of projections	1600
Exposure time per projection	0.5 s

III. Experiments and Results

A. Spatial Resolution Measurement of the Developed Imaging System

The spatial resolution of the developed system was characterized using the resolution test pattern (Xrnanotech, Switzerland). The modulation contrast was evaluated from a line profile drawn perpendicular to five 1-µm-wide Au lines arranged with a 2-µm pitch. The measured modulation contrast was 0.283, which exceeded the 0.2 criterion, indicating a spatial resolution of sub-µm [15].

This demonstrates that, despite the use of a high-power X-ray tube whose focal spot is two orders of magnitude larger than the target resolution, geometric blur from the source is effectively eliminated by the optical-coupling configuration, and the achievable resolution is set by the optical lens and the detector sampling rather than by the X-ray source.

B. 3D Imaging of an HBM Module

To evaluate the 3D imaging performance of the developed system on a realistic device, a packaged HBM module containing multiple stacked DRAM dies on a base logic die was inspected. 1600 2D projection images were acquired according to the parameters listed in Table I and were reconstructed into a 3D volume using the filtered back-projection (FBP) algorithm implemented in the ASTRA Toolbox [16]. The reconstruction grid was chosen to match the effective pixel size at the object plane, so that the in-plane voxel size was approximately 0.64 µm. The FBP reconstruction of the full 3D volume took approximately 10 minutes on an NVIDIA RTX 5090 GPU.

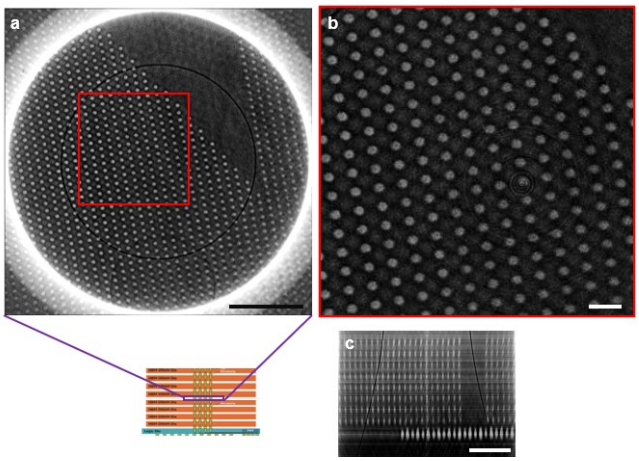


Figure 4. Reconstructed 3D images of an HBM2 package.
(a) In-plane slice of the micro-bump layer located between adjacent DRAM dies. Scale bar 400 µm.
(b) Magnified view of the boxed region in (a), showing the micro-bump array. A representative bump void is indicated. Scale bar 50 µm.
(c) Cross-sectional view of the HBM2 package showing the stacked micro-bump interconnections. Scale bar 200 µm.

Fig. 4 shows representative cross-sectional slices and a 3D rendering of the reconstructed HBM volume. The horizontal (x–y) slices clearly resolve the regular two-dimensional array of micro-bumps located both between adjacent DRAM dies and between the lowest DRAM die and the underlying logic die. Individual bumps are clearly separated from

neighboring bumps, and the bump diameters and pitches are consistent with the design specifications of the inspected HBM module. In the magnified inset, an isolated bright region inside one of the bumps reveals a clear bump void, demonstrating that the spatial resolution and contrast of the system are sufficient for detection of typical bonding defects in HBM.

The reconstructed cross-sections also exhibit the expected anisotropy in spatial resolution that is characteristic of computed laminography: the in-plane (x–y) resolution is essentially diffraction- and pixel-limited, while the axial (z) resolution is degraded by the so-called missing-cone region in the Fourier-space sampling of CL acquisitions [17]. For HBM inspection, however, the geometry was deliberately chosen so that the DRAM stack layers were aligned parallel to the x–y inspection plane. As a result, defects of interest such as bump voids, bump misalignment, and local non-wets, which are best visualized in the x–y plane that contains the bump array, are resolved with the high in-plane resolution of the optical system, while the limited z-resolution is sufficient to distinguish individual DRAM-to-DRAM and DRAM-to-logic bump layers.

Compared with conventional micro-focus CT systems, which typically require more than 30 minutes to acquire a high-resolution 3D image of a comparable HBM volume, the present optically-coupled X-ray CL system completed acquisition under 30 minutes for the parameter set used in this work, and additional reductions are accessible by further increasing the X-ray tube power, shortening the per-projection exposure, or reducing the number of projections at the cost of moderate noise increase. These results indicate that the proposed configuration is well aligned with the throughput requirements of in-line HBM inspection.

IV. Conclusion

An optically-coupled X-ray computed laminography system has been developed for high-speed, high-resolution 3D inspection of high-bandwidth memory modules. By placing a thin CsI:Tl scintillator in direct contact with the object and acquiring images through a 10× objective lens, the geometric magnification factor is made nearly unity, so that the focal spot size of the X-ray source is decoupled from the achievable spatial resolution. This allows a high-power X-ray tube to be used without compromising image quality, which removes the long-standing trade-off between resolution and scan time that constrains conventional micro-focus CT-based HBM inspection.

The developed system achieved an effective pixel size of 0.64 μm at the object plane and a measured limiting resolution near 1 μm. Three-dimensional reconstruction of a packaged HBM module from 1600 projections clearly resolved DRAM-to-DRAM and DRAM-to-logic micro-bumps and revealed bump voids, demonstrating that the resolution and contrast of the system are sufficient for detection of representative bonding defects. Because the underlying configuration is compatible with high X-ray tube power and short exposures, the proposed approach provides a practical route toward high-speed, high-resolution 3D inspection of advanced HBM packages, and it can be extended to other 2.5D/3D advanced packages and to a broader range of planar high-aspect-ratio samples.

Acknowledgment

This work was supported by the National Research Foundation of Korea (NRF) grant funded by the Korea government (MSIT) (RS-2025-25394640).

References

[1] J. H. Kim and S. K. Lim, "Architectural and Packaging Trends in High-Bandwidth Memory for AI and HPC Applications," Proceedings of the IEEE International Electron Devices Meeting (IEDM), pp. 1–4, 2023.

[2] Y. Wang, et al., "Defect Analysis in Through-Silicon-Via (TSV) Based 3D IC Packaging," Microelectronics Reliability, Vol. 124, pp. 114289, 2021.

[3] S. K. Kang, et al., "Reliability Challenges of Micro-Bump Interconnects in 2.5D/3D Packages," Proceedings of the Electronic Components and Technology Conference (ECTC), pp. 1547–1554, 2020.

[4] H. Villarraga-Gómez, D. L. Begun, P. Bhattad, K. Mo, M. Norouzi Rad, R. T. White, and S. T. Kelly, "X-ray Computed Tomography for Semiconductor Packaging Inspection," Nondestructive Testing and Evaluation, Vol. 37, pp. 519–544, 2022.

[5] S. Carmignato, W. Dewulf, and R. Leach, "X-ray Computed Tomography," in Precision Metal Additive Manufacturing, CRC Press, Chapter 12, pp. 313–346, 2020.

[6] R. Behling, C. Hulme, P. Tolias, and M. Danielsson, "Thermal Limits of X-ray Tube Targets," Medical Physics, Vol. 52, pp. 814–830, 2025.

[7] J. Im, J. Heo, S. Cheon, J. Kim, and S. O. Cho, "Optically-Coupled X-Ray Computed Laminography System for High-Speed Inspection of Lithium-Ion Batteries," Advanced Science, Vol. 13, e17158, 2026.

[8] F. Xu, L. Helfen, T. Baumbach, and H. Suhonen, "Comparison of Image Quality in Computed Laminography and Tomography," Optics Express, Vol. 20, No. 2, pp. 794–806, 2012.

[9] J. Hiller, M. Maisl, and L. M. Reindl, "Physical Characterization and Performance Evaluation of an X-ray Micro-Computed Tomography System for Dimensional Metrology," Measurement Science and Technology, Vol. 23, p. 085404, 2012.

[10] T. E. Gureyev, Y. I. Nesterets, A. W. Stevenson, P. R. Miller, A. Pogany, and S. W. Wilkins, "A Method for Local Phase Retrieval in X-ray Imaging," Optics Express, Vol. 16, pp. 3223–3241, 2008.

[11] Lord Rayleigh, "On the Manufacture and Theory of Diffraction Gratings," Philosophical Magazine, Vol. 47, pp. 81–93, 1874.

[12] R. K. Swank, "Absorption and Noise in X-ray Phosphors," Applied Optics, Vol. 12, No. 8, pp. 1865–1870, 1973.

[13] D. M. Levi and S. A. Klein, "Equivalent Intrinsic Blur in Spatial Vision," Vision Research, Vol. 30, pp. 1971–1993, 1990.

[14] G. Li, S. Luo, Y. Yan, and N. Gu, "A method of extending the depth of focus of the high-resolution X-ray imaging system employing optical lens and scintillator: a phantom study," BioMedical Engineering OnLine, Vol. 14, Suppl. 1, p. S15, 2015.

[15] M. Modrzejewski, A. Bjeoumikhov, S. Bjeoumikhova, M. Radtke, "Road to micron resolution with a color X-ray camera — polycapillary optics characterization," J. Anal. At. Spectrom., vol. 34, no. 3, pp. 489-498, 2019.

[16] W. van Aarle, et al., "The ASTRA Toolbox: A Platform for Advanced Algorithm Development in Electron Tomography," Ultramicroscopy, Vol. 157, pp. 35–47, 2015.

[17] L. Helfen, T. Baumbach, P. Mikulík, D. Kiel, P. Pernot, P. Cloetens, and J. Baruchel, "High-Resolution Three-Dimensional Imaging of Flat Objects by Synchrotron-Radiation Computed Laminography," Applied Physics Letters, Vol. 86, p. 071915, 2005